Miguel Angel Ariza-Gracia*, Matteo Friggelli, Malavika Nambiar, Abhijit Roy, Kevin Vallotton, Theo Seiler, and Philippe Büchler

Patient-Specific Finite Element Modeling of Refractive Surgery Biomechanics: Technical Assessment of PRK, LASIK, and KLEx

https://doi.org/10.1515/cdbme-2025-0130

Abstract: This study evaluates the biomechanical and optical consequences of three corneal refractive surgeries—PRK, LASIK, and KLEx—using patient-specific finite element simulations. Personalized corneal geometries were derived from preoperative tomography of 30 patients and subjected to virtual interventions modeled in a nonlinear anisotropic framework. Material parameters were calibrated from experimental human corneal data. Stress distributions and refractive outcomes were computed under physiological intraocular pressure. Despite identical tissue removal volumes, PRK preserved a more uniform stress distribution and delivered the least optical undercorrection. LASIK induced significant posterior stromal stress and KLEx, although mechanically intermediate, exhibited greater undercorrection due to cap-induced tension. The results support the integration of biomechanics-informed modeling in refractive surgery planning.

Keywords: Refractive surgery, finite element modeling, corneal biomechanics, optobiomechanics.

1 Introduction

The prevalence of refractive errors, particularly myopia, has escalated dramatically over the past two decades, with projections estimating that nearly half of the world's population will be affected by 2050 [1]. This surge has driven widespread demand for corneal refractive procedures aimed at reducing dependency on corrective lenses and improving uncorrected visual acuity. Among these, photorefractive keratectomy (PRK), laser-assisted in situ keratomileusis (LASIK), and keratorefractive lenticule extraction (KLEx; marketed under various commercial names as SMILE, CLEAR, or SmartSight) are the most common techniques.

Despite their optical efficacy, these procedures inherently alter the cornea's biomechanical stability. Tissue removal or separation modifies stress distributions, influencing long-term shape and refractive predictability. However, current surgical planning systems rely on empirically derived nomograms that inadequately capture patient-specific biomechanical behavior. Finite element (FE) modeling offers a solution by enabling personalized assessment of post-surgical deformation and mechanical integrity.

This study presents a technical comparison of PRK, LASIK, and KLEx using individualized FE simulations that integrate nonlinear anisotropic corneal properties. By systematically evaluating mechanical stress distributions and optical outcomes in 30 patients, we aim to highlight the biomechanical distinctions between procedures and propose mechanical correction factors to enhance refractive accuracy.

2 Methods

2.1 Patient Geometry and Meshing

A surface mesh representing the anterior and posterior corneal surfaces was constructed for each of the 30 patients using elevation profiles obtained from Pentacam HR tomography. The epithelium was modeled as a uniform 53 µm thick layer across all patients. As the epithelium does not contribute to the cornea's biomechanical stiffness, it was excluded from the finite element simulations but reintroduced

***Corresponding author: Miguel A. Ariza-Gracia:** ARTORG, University of Bern, Freiburgstrasse 3, 3010, Bern, Switzerland, e-mail: miguel.ariza@unibe.ch
Matteo Frigelli, Malavika Nambiar: ARTORG, University of Bern, Bern, Switzerland.
Abhijit Roy: Narayana Nethralaya Eye Clinic, Bengaluru, India.
Kevin Vallottont, Theo Seiler: Universitätsklinik für Augenheilkunde, Inselspital Bern, Bern, Switzerland.
Philippe Büchler: ARTORG, University of Bern, Bern, Switzerland.

afterward for accurate optical assessments. This was achieved by shifting the anterior surface by 53 µm posteriorly for mechanical simulations and restoring it after deformation to compute curvature and refraction maps.

Each patient's dataset was used to generate four finite element models: one preoperative configuration and three representing PRK, LASIK, and KLEx, respectively. All surgical profiles were based on clinical planning data, incorporating individualized parameters such as cap/flap thickness (110 µm), optical zone (6 mm), ablation zone (7.9 mm), and refractive correction values in sphere and cylinder.

The Mrochen formula was used to compute the ablation or lenticule volume for each procedure [2]. In PRK, ablation was simulated on the anterior corneal surface. LASIK and KLEx involved tissue removal at a fixed depth of 110 µm, with LASIK including a flap mesh and KLEx a lenticule pocket. Both LASIK and KLEx models used nonlinear penalty contact to enforce interaction between tissue interfaces without allowing separation under load.

All meshes were generated using GMSH through a Python-based automation pipeline, resulting in structured hexahedral meshes composed of ~80,000 linear elements per model. A physiological intraocular pressure of 15 mmHg was applied to the posterior corneal surface. At the limbus, a sliding boundary condition allowed radial displacements in a spherical coordinate system while constraining angular rotations.

2.2 Material Model

The corneal stroma was modeled using a hyperelastic, anisotropic Holzapfel-Gasser-Ogden formulation incorporating fiber dispersion. This model accounts for collagen fiber orientation and nonlinear tension response using angular integration of fiber density in spherical coordinates. The model parameters were previously calibrated and published by our group based on experimental data from uniaxial testing of human corneal strips at varying stromal depths. [3].

$$U = C_{10}(\bar{I}_1 - 3) + \int_0^{\pi}\int_0^{2\pi} \rho(\varphi,\theta)\left\{\frac{k_1}{2k_2}\{\exp[k_2 < \bar{E} >^2] - 1\}\right\}\sin\theta \, d\theta d\varphi$$

$$\bar{E} = \bar{I}_4(\mathbf{a}) - 1 - f_c$$

where C_{10}, k_1, k_2 and f_c are material parameters, and $\bar{I}_1$ and $\bar{I}_4$ are invariants of the isochoric Cauchy-Green strain tensor. $\rho(\varphi,\theta)$ is the is the angular density of the fiber distribution in spherical coordinate system, decomposed as a product of the in-plane $\rho_{ip}(\varphi)$ and out-of-plane distributions $\rho_{op}(\theta)$:

$$\rho(\varphi,\theta) = \rho_{op}(\theta)\rho_{ip}(\varphi)$$

$$\rho_{op}(\theta) = 2\sqrt{\frac{2b}{\pi}}\frac{\exp[-2b\cos^2\theta]}{\mathrm{erf}(\sqrt{2b})},\ 0 \le \theta \le \pi$$

$$\rho_{ip}(\varphi) = \frac{\exp[a\cos 2\varphi]}{I_0(a)},\ 0 \le \varphi \le 2\pi$$

The model incorporated depth-dependent mechanical behavior. The stiffness parameter decreased linearly from anterior to posterior stroma, while the fiber dispersion parameter increased. The anterior stroma was modeled as isotropic (a = 0), transitioning to aligned nasal-temporal collagen orientation (a = 5) in the posterior third. A sigmoid function was used to model this transition, while the out-of-plane alignment parameter (b = 2.5) was kept constant.

To identify material constants, an optimization algorithm was employed to fit experimental force-displacement curves. Validation was performed by reproducing uniaxial tests on human lenticules obtained during KLEx surgery and matching inflation response data from prior studies [3,4].

Table 1: Depth-dependent mechanical properties of the cornea. The mechanical parameters of the mechanical model of the cornea were identified using depth-dependent experimental data. The mechanical parameter k_1 and the in-plane fiber dispersion parameter a were continuously varied across the corneal depth between their values at the anterior and posterior surfaces.

C_{10}	38 (kPa)
k_1 anterior	3.46 (MPa)
k_1 posterior	1.10 (MPa)
k_2	21.0 (-)
a anterior	0 (-)
a posterior	5 (-)
b	2.5 (-)
f_c	0.02 (-)

2.3 Surgical Simulation

A three-stage simulation pipeline was implemented. First, a preoperative model incorporating depth-dependent material properties was generated. A stress-free configuration was computed via an iterative algorithm to account for residual stresses that are not directly measurable but influence baseline geometry under physiological loading [6].

This stress-free geometry was then mapped onto three modified meshes representing PRK, LASIK, and KLEx. Surgical modifications were implemented by altering the element geometry according to the computed ablation or lenticule profile and introducing the appropriate flap or cap features.

In LASIK and KLEx, nonlinear contact elements were introduced to model the interface behavior post-ablation. PRK, lacking such separations, maintained continuous stress distribution through the stroma. The IOP of 15 mmHg was reapplied to the modified models to simulate the postoperative state.

2.4 Optical and Biomechanical Analysis

The deformed corneal shape from each simulation was analyzed to extract the anterior curvature profile. From this, objective refractive parameters—sphere, cylinder, and astigmatism axis—were calculated using paraxial optics approximations. These values were compared to the intended correction defined by the surgical planning using the Mrochen algorithm [2].

Mechanical evaluation included computation of the maximum principal stress distributions across the corneal thickness, with specific attention to the location and magnitude of peak stress. Differences in stress patterns across procedures were used to assess biomechanical preservation and structural redistribution.

Additionally, a mechanical correction factor was derived for each surgical type. This factor quantifies the discrepancy between intended and achieved corrections and provides a scale to adjust surgical planning inputs. Separate factors were computed for spherical and cylindrical corrections across all three techniques, enabling compensation for biomechanical deformation during tissue removal.

3 Results

The validated mechanical model parameters accurately reproduced corneal tissue behavior across various depths [3]. The maximum principal stress in the presurgical cornea of the 30 patients had an average value of 15.1 ± 1.4 kPa. LASIK produced the highest increase in maximum principal stress (maximum principal stress of 23.0 ± 2.9 kPa; 53% ± 16% increase w.r.t. presurgical stress), followed by KLEx (21.7 ± 3.0 kPa; increase of 44% ± 18%), and PRK

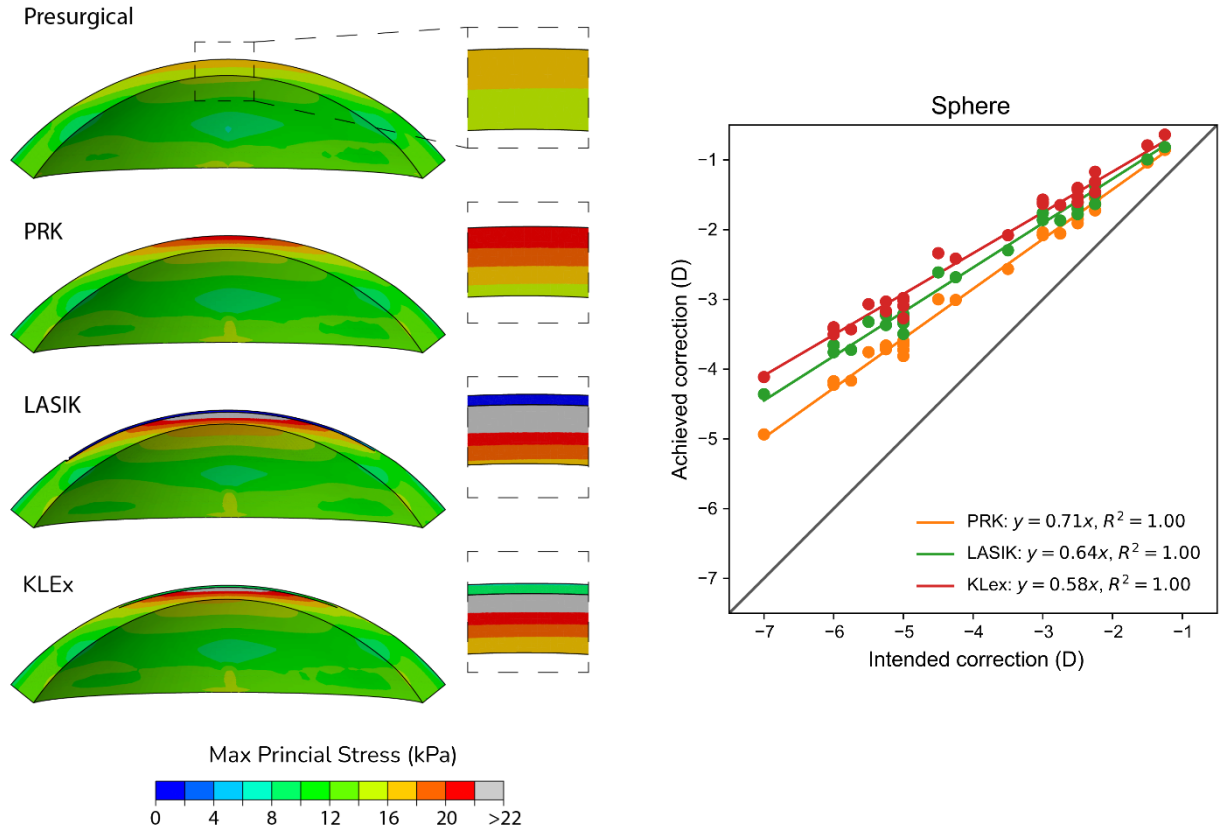

Figure 1: Comparison of stress distribution and refractive outcomes following PRK, LASIK, and KLEx procedures. (Left) Cross-sectional views of the cornea, highlighting increased post-surgical stress levels. (Right) Correlation between achieved and target spherical correction, indicating undercorrection patterns for each procedure.

(19.4 ± 2.3 kPa; increase of 28% ± 12%). PRK maintained anterior stress distribution, whereas LASIK and KLEx shifted stress posteriorly, leaving the flap and cap with minimal load-bearing roles.

All three techniques exhibited consistent refractive undercorrection, which increased linearly with the target correction magnitude. For a 7D spherical correction, undercorrection exceeded 2D in LASIK and KLEx, while PRK resulted in the lowest deviation. Cylinder undercorrection was also smallest in PRK, with axis orientation unaffected across procedures.

Correction factors derived from regression between intended and achieved values revealed the need to scale manifest refractions. For spherical corrections, multipliers were 1.40 (PRK), 1.57 (LASIK), and 1.71 (KLEx). For cylindrical corrections, they were 1.11, 1.18, and 1.23, respectively. These factors translated into ablation depth increases of up to 49 µm when accounting for biomechanical effects.

4 Discussion

Our findings show that mechanical weakening from refractive surgery significantly alters optical outcomes, particularly under physiological IOP. Although KLEx is less invasive than LASIK in terms of incision geometry, the tension in the cap introduces mechanical mismatch, leading to more severe undercorrection.

In PRK, tissue removal occurs without structural decoupling, preserving anterior load-bearing regions. LASIK, in contrast, creates a non-load-bearing flap that limits structural resistance. KLEx creates a cap that resists deformation, leading to suboptimal conformity and elevated optical error.

These insights extend previous findings that PRK better preserves corneal stiffness [8] and confirm that surgical geometry—not just tissue volume—drives postoperative behavior. Personalized FE modeling could therefore guide patient-specific procedure selection and improve nomogram calibration.

Furthermore, the correction factors derived from simulation outcomes offer a quantitative method to compensate for biomechanical discrepancies in surgical planning. Rather than applying a uniform nomogram across all procedures, tailored adjustments could be incorporated to align surgical intent with biomechanical response.

Limitations of this study include the exclusion of epithelial remodeling and wound healing, which can affect long-term refractive outcomes. The influence of dynamic IOP fluctuations, hydration gradients, and patient-specific healing profiles warrant further investigation. Future work should aim to integrate such physiological variables and validate simulation outputs with longitudinal clinical follow-up.

5 Conclusion

Patient-specific finite element simulations revealed that PRK results in superior biomechanical and refractive outcomes compared to LASIK and KLEx. Incorporating depth-dependent anisotropic material behavior and nonlinear contact interactions, our models provided individualized predictions of postoperative stress and refraction. The introduction of correction factors based on mechanical behavior offers a pathway toward improved planning and safety in refractive surgery.

Author Statement

Research funding: This study was funded by the Swiss National Science Foundation, Switzerland (IZLIZ3_182975).

Conflict of interest: The authors declare no conflict of interest.

Informed consent: Informed consent has been obtained from all individuals included in this study.

Ethical approval: The research related to human use complies with all relevant national regulations and institutional policies, was performed in accordance with the tenets of the Helsinki Declaration, and has been approved by the authors' institutional review board (Ethics number: 2018-01552).

References

[1] Holden BA, Fricke TR, Wilson DA, et al. *Global prevalence of myopia and high myopia and temporal trends from 2000 through 2050*. Ophthalmology. 2016;123(5):1036-1042.

[2] Mrochen M, Kaemmerer M, Seiler T. *Wavefront-optimized ablation profiles: Theoretical background*. J Cataract Refract Surg. 2004;30(4):804-811.

[3] Nambiar MH, Seiler TG, Senti S,et al.. *Depth-dependent mechanical properties of the human cornea by uniaxial extension*. Exp Eye Res. 2023;237:109718.

[4] Nambiar MH, Roy AS, Büchler P. *Anisotropic finite element modeling of the human cornea for personalized refractive surgery planning*. J Mech Behav Biomed Mater. 2023;147:106141.

[5] Ariza-Gracia MA, Llorens D, Calvo B, et al. *Coupled modeling of the pre-stressed human cornea and air–tear film interaction during blinking*. PLoS One. 2015;10(3):e0121486.

[6] Santhiago MR, Smadja D, Wilson SE, et al. *Tissue Altered on Ectasia After LASIK in Eyes With Suspicious Topography*. J Refract Surg. 2015;31(4):258-265.